Available online at www.sciencedirect.com

SciVerse ScienceDirect

Geochimica et Cosmochimica Acta 77 (2012) 186–201

Geochimica et Cosmochimica Acta

www.elsevier.com/locate/gca

Towards constraining H_2 concentration in subseafloor sediment: A proposal for combined analysis by two distinct approaches

Yu-Shih Lin [a,b,*], Verena B. Heuer [a,b], Tobias Goldhammer [b], Matthias Y. Kellermann [a,b], Matthias Zabel [b], Kai-Uwe Hinrichs [a,b]

[a] Organic Geochemistry Group, Department of Geosciences, University of Bremen, 28359 Bremen, Germany
[b] MARUM Center for Marine Environmental Sciences, University of Bremen, 28359 Bremen, Germany

Received 5 November 2010; accepted in revised form 1 November 2011; available online 9 November 2011

Abstract

Molecular hydrogen (H_2) is a central metabolite that couples organic matter degradation and terminal electron-accepting processes. H_2 levels in natural environments are often regulated by microbial syntrophy; therefore, pore-water H_2 concentration is a useful parameter for studying biogeochemical processes in sediments. However, little is known about H_2 concentrations in marine subsurface sediments. Previous studies applying either a headspace equilibration technique or an extraction method for the analysis of pore-water H_2 in deeply buried sediments have generated results that sometimes contradict the principles established based on studies of microbial culture and surface sediments. In this study, we first evaluated and optimized an extraction method, which was then applied in combination with a headspace equilibration method to determine concentrations of pore-water H_2 in subseafloor sediments along a transect of five sites of different water depths and geochemical regimes at the continental margin off Namibia, SE Atlantic. The two methods generated depth profiles with some similarities in curve shape, but the extraction method yielded higher H_2 values than the headspace equilibration technique. By comparing the two data sets with thermodynamic calculations of potential terminal electron-accepting processes, we were able to provide a first evaluation of syntrophic conditions in subseafloor sediment from the perspective of H_2 biogeochemistry. We observed that in the sulfate reduction zone, the H_2 concentrations are higher than the H_2 threshold allowed for the next most favorable terminal metabolism (methanogenesis), suggesting relaxation of coupling between H_2-producing and H_2-consuming activities at these depths. In contrast, the H_2 concentrations in the upper methanogenic zone are low enough for methanogens to outcompete CO_2-reducing acetogens. Our findings suggest the existence of varied extents of syntrophic H_2 coupling in subseafloor sediment.

1. INTRODUCTION

Marine sediments contain one of the largest reservoirs of organic carbon on Earth (Hedges and Keil, 1995) and maintain a subseafloor biosphere consisting of viable (Schippers et al., 2005), ubiquitous (Teske, 2006), diversity-limited (Inagaki et al., 2006), and mostly uncultured prokaryotes with poorly understood physiologies and activities. Downcore distributions of redox-related chemical species suggest the presence of ongoing terminal electron-accepting processes; however, the metabolic rates are several orders of magnitude lower than those detected in surface ecosystems (D'Hondt et al., 2002). The stable carbon isotope biogeochemistry of low-molecular-weight metabolites provides additional evidence for the ongoing degradation of organic matter and for the reduction of dissolved inorganic carbon (DIC) to both methane and acetate in deep subsurface sediments (Heuer et al., 2009; Pohlman

* Corresponding author at: MARUM Center for Marine Environmental Sciences, University of Bremen, Leobener Str., Room 2610, 28359 Bremen, Germany. Tel.: +49 421 218 65744; fax: +49 421 218 65715.
E-mail address: yushih@uni-bremen.de (Y.-S. Lin).

0016-7037/$ - see front matter © 2011 Elsevier Ltd. All rights reserved.
doi:10.1016/j.gca.2011.11.008

et al., 2009; Lever et al., 2010). However, the role of molecular hydrogen (H_2), a key metabolite that links organic matter degradation to terminal electron-accepting processes, remains poorly constrained.

H_2 in marine sediments can be supplied by at least the following three processes. (1) H_2 is generated during fermentation and thermal alteration of sedimentary organic matter (Hoehler et al., 1998; Seewald, 2003). (2) Abiotic H_2 production via serpentinization has been proposed to sustain ecosystems in hydrothermal fields (e.g., Kelley et al., 2005). Geochemical evidence suggests that serpentinization also takes place in deep sediments near the décollement (Spivack et al., 2002), although no corresponding H_2 data have been published. (3) Radiolysis of water is a ubiquitous process that supplies H_2 (D'Hondt et al., 2009). Its relative contribution increases significantly in organic-poor sediment (Blair et al., 2007). In addition, pyrite precipitation is also known to generate H_2 under anoxic conditions (Drobner et al., 1990), but its contribution in marine sediment has not been investigated. On the other hand, the ability to utilize H_2 is a common feature of various microorganisms that use different electron acceptors, including oxygen (O_2), Fe(III), Mn(IV), sulfate (SO_4^{2-}), carbon dioxide (CO_2), and several low-molecular-weight organic compounds (Cord-Ruwisch et al., 1988).

Microbial H_2 production and consumption are often closely coupled via interspecies hydrogen transfer in syntrophic relationships (for recent reviews see Schink and Stams, 2006; Stams and Plugge, 2009). The following principles have been established in studies of microbial cultures. (1) When fermenting bacteria are cultured alone, H_2 generation eventually becomes inhibited by product accumulation. (2) The inhibition by H_2 accumulation can be overcome when fermenting bacteria are co-cultured with H_2 consumers to form a syntrophic consortium. Decrease of H_2 in such a consortium finally levels off with H_2 reaching a threshold concentration, and the corresponding Gibbs free energy (ΔG) values of the H_2 consuming reactions have been considered as the minimal amount of energy needed to sustain life (Schink and Stams, 2006). (3) H_2 thresholds vary among different types of anaerobic respiration and usually increase with decreasing redox potential, for example in the order of nitrate reduction < iron and manganese reduction < sulfate reduction < methanogenesis (Table 1). (4) H_2 thresholds are temperature dependent, in agreement with predictions by thermodynamics (Conrad and Wetter, 1990). In summary, the close relationship between H_2 concentrations and microbial syntrophy makes H_2 a particularly attractive parameter for studying anaerobic microbial communities in marine sediments.

In studies of microbial cultures, H_2 thresholds of syntrophic relationships have typically been investigated by a headspace equilibration method (e.g., Cord-Ruwisch et al., 1988). In this method, gaseous H_2 is analyzed in a headspace that is in equilibrium with dissolved H_2 while samples are incubated for periods that ensure the establishment of a steady state between the production and consumption of H_2. At steady state, close coupling dictates that H_2 concentrations are governed by the thermodynamics of H_2-consuming reactions (Cord-Ruwisch et al., 1988). When applied to shallow sediments (Lovley and Goodwin, 1988; Hoehler et al., 1998), this method yielded H_2 concentrations that matched excellently with predicted H_2 thresholds obtained from culture studies (Table 1). Furthermore, the H_2 concentrations maintained during a given mode of terminal metabolism were found to be low enough to restrain the next most favorable process, suggesting thermodynamic control on H_2 concentrations in real world situations (Hoehler et al., 1998, 2001).

However, when the same approach was first applied to subseafloor sediments retrieved during the Ocean Drilling Program (ODP) Leg 201 at the Peru margin (D'Hondt et al., 2003), the measured H_2 concentrations did not always agree with the thermodynamically predicted values. One extreme example is ODP Site 1231, where pore waters are rich in sulfate till the bottom of the cores (~110 m below the seafloor). Nevertheless, pore-water H_2 reached concentrations of 29–102 nmol L^{-1} in the top 20–30 m, thus greatly exceeding the threshold concentrations for sulfate reduction and reaching levels at which even reductive methanogenesis can be a sufficient energy-yielding reaction. There were also sediments in which H_2 concentrations were much lower than values predicted by thermodynamics. For example, in the deep methanogenic zone at ODP Site 1229, H_2 concentrations were mostly below 1 nmol L^{-1}, while CO_2 reduction to methane would have required a H_2 concentration of 2–4 nmol L^{-1}.

The disagreement between thermodynamically predicted and measured H_2 concentrations in subseafloor sediments, as observed during ODP Leg 201, raises the question whether the headspace equilibration method and the underlying model of closely coupled syntrophic relationships fail because: (1) close H_2 coupling of syntrophic partners is present in situ but cannot be established quickly enough in vitro to support the headspace equilibration method. This is conceivable based on the low microbial activities in subseafloor sediment (D'Hondt et al., 2002). Loss of microbial activities due to depressurization during core retrieval or inappropriate incubation conditions may also contribute to the mismatch. (2) Alternatively, close H_2 coupling of syntrophic partners is present neither in vitro nor in situ. Theoretically, these two hypotheses can be tested when the headspace equilibration method is combined with direct analysis of pore-water H_2. For example, if the value obtained by headspace equilibration in vitro ($[H_2]_{INC}$) is much higher than the thermodynamically predicted threshold concentration of H_2 ($[H_2]_{TD}$) (as observed at ODP Site 1231; D'Hondt et al., 2003), a concentration of directly extracted H_2 ($[H_2]_{EXT}$) lower than $[H_2]_{INC}$ and similar to $[H_2]_{TD}$ would support hypothesis 1. On the contrary, a $[H_2]_{EXT}$ higher than $[H_2]_{TD}$ and approaching $[H_2]_{INC}$ would support hypothesis 2.

To date, no method is available for reliable direct determination of H_2 concentrations in pore-water. Most published methods for determining $[H_2]_{EXT}$ involve an extraction step in which a sediment slurry is equilibrated with a H_2-free headspace (e.g., Conrad et al., 1985; Novelli et al., 1987; D'Hondt et al., 2009). This approach avoids incubation, which may generate both biological and chemical artifacts. However, it is also known to bear the following limitations. (1) Extraction methods suffer from

Table 1
Comparison of threshold H_2 values in cultures, steady-state H_2 concentrations in environmental samples based on the headspace equilibration technique, and in situ H_2 concentrations determined by extraction methods.

Redox process	Type of culture or sediment sample	Method[a]	T (°C)[b]	Dissolved H_2 (nmol L^{-1})[c]	Ref.[d]
Oxygen reduction	Knallgas bacteria	A: $[H_2]_{INC}$	20–30	0.5–6.2	1, 2
	Marine sediment (off Baja, Mexico)	C: $[H_2]_{EXT}$	2–4	<LoD (11)	3
	Subseafloor sediment (South Pacific Gyre)	C: $[H_2]_{EXT}$	2–4	<LoD (2–229)	4
Nitrate reduction	Nitrate reducing bacteria	A: $[H_2]_{INC}$	28–34	<0.05	5
	Freshwater sediment (Potomac River, MD, USA)	A: $[H_2]_{INC}$	20	<0.05	6
	Marine sediment (Cape Lookout Bight, NC, USA)	A: $[H_2]_{INC}$	25	0.03	7
Mn(IV) reduction	Mn(IV) reducing bacteria	A: $[H_2]_{INC}$	30	0.3	8
	Freshwater sediment (Potomac River, MD, USA)	A: $[H_2]_{INC}$	20	<0.05	6
	Marine sediment (Cape Lookout Bight, NC, USA)	A: $[H_2]_{INC}$	25	~2	7
Fe(III) reduction	Fe(III) reducing bacteria	A: $[H_2]_{INC}$	20–30	0.3–0.6	8, 9
	Freshwater sediment (Potomac River, MD, USA)	A: $[H_2]_{INC}$	20	0.2	6
	Marine sediment (Cape Lookout Bight, NC, USA)	A: $[H_2]_{INC}$	25	~2	7
Sulfate reduction	Sulfate reducing bacteria	A: $[H_2]_{INC}$	28–34	2–13	5, 10
	Freshwater sediment (Potomac River, MD, USA)	A: $[H_2]_{INC}$	20	1–1.5	6
	Marine sediment (Cape Lookout Bight, NC, USA)	B: $[H_2]_{INC}$	25	1.6	7
	Marine sediment (Town Cove, MA, USA)	C: $[H_2]_{EXT}$	20	<10	11
	Marine sediment (Buzzards Bay, MA, USA)	C: $[H_2]_{EXT}$	20	2–25	11
	Marine sediment (Princess Louisa Inlet, BC, Canada)	C: $[H_2]_{EXT}$	6	2–25	3
	Estuary sediment (Carmans River Estuary, NY, USA)	C: $[H_2]_{EXT}$	NA	20–30	12
Methanogenesis	Methanogens	A: $[H_2]_{INC}$	28–39	6–70	5, 13, 14
	Freshwater sediment (Potomac River, MD, USA)	A: $[H_2]_{INC}$	20	7–10	6
	Marine sediment (Cape Lookout Bight, NC, USA)	B: $[H_2]_{INC}$	25	13	7
	Freshwater sediment (Lake Mendota, WI, USA)	C: $[H_2]_{EXT}$	8	20–40	15
	Marine sediment (Skan Bay, AK, USA)	C: $[H_2]_{EXT}$	4	40–60	3
	Estuary sediment (Carmans River Estuary, NY, USA)	C: $[H_2]_{EXT}$	NA	100–290	12
Acetogenesis	Acetogens	A: $[H_2]_{INC}$	28–34	70–1300	5, 10, 14
	Marine sediments (Cape Lookout Bight, NC, USA)	B: $[H_2]_{INC}$	20–25	117–150	9

[a] Methods: A: $[H_2]_{INC}$ = headspace equilibration technique with addition of substrates; B: $[H_2]_{INC}$ = headspace equilibration technique without addition of substrates; C: $[H_2]_{EXT}$ = extraction methods.
[b] The incubation temperatures for the headspace equilibration technique and the in situ temperatures of the samples investigated by the extraction methods. NA: temperature data not available.
[c] When the original data for isolates were presented in the unit of molar fraction or Pa, we converted the values into dissolved concentration (nmol L^{-1}) according to the data of pressure, temperature and salinity described in the articles. LoD: limit of detection.
[d] References: 1 = Conrad et al. (1983); 2 = Häring and Conrad (1991); 3 = Novelli et al. (1987); 4 = D'Hondt et al. (2009); 5 = Cord-Ruwisch et al. (1988); 6 = Lovley and Goodwin (1988); 7 = Hoehler et al. (1998); 8 = Lovley et al. (1989); 9 = Klüber and Conrad (1993); 10 = Krumholz et al. (1999); 11 = Novelli et al. (1988); 12 = Michener et al. (1988); 13 = Lovley (1985); 14 = Kotsyurbenko et al. (2001); 15 = Conrad et al. (1985); 16 = Hoehler et al. (1999).

the presence of background H_2 which gives rise to high blanks and limits of detection (for definition of terms see Section 3.1.1). Novelli et al. (1987) reported a blank H_2 level of 10–14 nmol L^{-1}, whereas the method of D'Hondt et al. (2009) had a limit of detection (LoD) of 2–229 nmol L^{-1}. Given such a blank and LoD, the methods cannot always unambiguously detect thermodynamically controlled low concentrations of H_2 (Table 1), and $[H_2]_{EXT}$ in marine sediments can be expected to be largely below the LoD if concentrations were in fact governed by close coupling of microbial syntrophy. Currently, extraction methods can only identify a subset of all potential cases, in which H_2 coupling of syntrophic partners is present in situ, namely those involving H_2 consumption by methanogens and acetogens at room temperature (Table 1). In order to include further H_2-consuming processes, the extraction approach needs to be optimized for a lower and more reproducible LoD. Nevertheless, the extraction method allows identification of extreme cases in which $[H_2]_{EXT}$ is high because H_2 coupling of syntrophic partners is not present in situ. Examples of high $[H_2]_{EXT}$ above the LoD have been reported in the literature (Table 1). (2) For active systems where the residence time of H_2 is short relative to the equilibration period, extraction methods will cause an overestimation of H_2 values. This is because H_2 partitions preferentially into the gaseous phase. The removal of H_2 lowers the concentration of dissolved H_2 and results in excess H_2 production (Krämer and Conrad, 1993). While excess H_2 production can be a serious problem in very active microbial ecosystems, it is likely of minor importance in deep subseafloor sediments where microbial metabolism is known to be very slow.

This study seeks to improve the extraction approach for H_2 analysis in order to combine it with the established

incubation method (Hoehler et al., 1998) for investigating the H_2 coupling of syntrophic partners in subseafloor sediments. Aiming to optimize the extraction method, we performed laboratory experiments to diagnose the source of background H_2 interfering with sensitive analysis, evaluated the methodological LoD (LoD_m), and tested the optimized method using sediment samples. The optimized extraction method was combined with the headspace equilibration technique (Hoehler et al., 1998) and thermodynamic calculations to study H_2 in five subseafloor environments with different water depths and geochemical properties along a transect across the continental margin off Namibia, SE Atlantic. We demonstrate how the combined analysis of two distinct approaches enhances the reliability of the data sets, and discuss the extent of coupling between syntrophic partners in subseafloor sediments from the perspective of H_2 geochemistry.

2. MATERIALS AND METHODS

2.1. Sites

Sediment samples for method development were taken during expeditions M76/1 (April–May 2008) and M84/1 (February 2011) of the RV *Meteor*, and from a field trip to tidal flats of the coastal North Sea (November 2006). For evaluation of the optimized extraction method, three groups of samples were selected to account for conditions with low (Site GeoB 12803, Southeast Atlantic), intermediate (Site GeoB 15105 in the southwestern Black Sea) and high (Site GeoB 15101 in the Urania Basin and Site GeoB 15102 in the Discovery Basin, Mediterranean Sea) concentrations of dissolved H_2. To explore the distribution of H_2 in subseafloor sediments, downcore analysis of pore-water H_2 was performed during the expedition M76/1 using sediments collected from a transect across the continental margin off Namibia, SE Atlantic (Fig. 1; Table 2). At each site, sediments were sampled by a combination of multi-corer, which yielded an intact sediment/water interface and the upper 30–50 cm of sediment, and gravity corers, which enable recovery of the upper 6–12 m of sediment. All cores were processed and/or stored in a cold room at +4 °C within less than 1 h after retrieval. Subsamples for incubation experiments were stored under N_2 headspace at +4 °C. Gravity cores are archived at the MARUM core repository in Bremen.

2.2. Sampling

For analysis of gas and total organic carbon (TOC) content and for the determination of porosity, a subsample set of 2–3 mL sediment was collected by cut-off plastic syringes and transferred to glass vials. Vials were sealed and the exact sample volumes were recorded. In the case of multicorer cores, gas and solid phase sampling was conducted on deck immediately after core retrieval. The sediment was extruded from the core by measured increments and the freshly exposed sediment surface was sampled. In the case of gravity cores, syringe samples were first taken on deck when the core was cut into 1 m long segments.

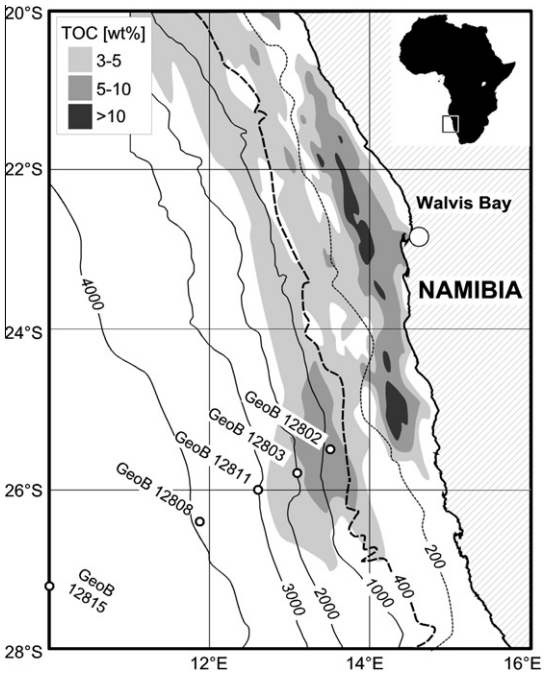

Fig. 1. Map of the continental margin off Namibia with the investigated stations from *Meteor* Expedition M76/1, 2008. Distribution of total organic carbon (TOC) adapted from Inthorn et al. (2006).

Samples were taken from each freshly cut segment base. To maximize the depth resolution, additional samples for gas analysis were taken at a later time, usually within a few hours, from intact whole round core segments that were stored in a cold room at +4 °C. Small ports (ca. 2 cm × 3 cm) were cut into the core liner and syringe samples were retrieved from the freshly exposed sediments. Our shipboard gas analyses showed that samples taken in the cold room gave generally comparable results to those taken on deck (see below).

Pore-water sampling was carried out while cores were stored in the cold room at +4 °C. For determination of dissolved inorganic species, interstitial water samples were extracted from intact whole round cores using Rhizon suction samplers (0.1 μm porous polymer, Rhizosphere Research, Wageningen, the Netherlands; Seeberg-Elverfeldt et al., 2005). Sampling was performed via small holes in the core liners. Pore-water samples for volatile fatty acids were obtained by a squeezer, using regenerated cellulose filters (Schleicher & Schuell, RC 58, 0.2 μm) and an overpressure applied by N_2 pressure tank. Pressure for extraction was 1.5–3 bar.

2.3. Analyses

2.3.1. Gas analysis

χ_{H_2}. The concentration of H_2 in headspace gases, expressed as mole fraction χ_{H_2}, was analyzed using a Peak Performer 1 gas chromatograph (Peak Laboratories, LLC, USA). Samples were injected into a flow of carrier gas and separated on a packed column before they reacted

Table 2
Location, water depth, and hydrostatic pressure at the seafloor of the stations and the total organic carbon (TOC) content of the sediments.

Station	Longitude (°E)	Latitude (°S)	Water depth (m)	Hydrostatic pressure at seafloor (Mpa)	TOC (wt%)[a]
GeoB 12802	13.45	25.50	791	8.1	7.4 ± 1.9
GeoB 12803	13.07	25.77	1944	19.6	6.6 ± 1.0
GeoB 12808	11.90	26.37	3796	38.3	1.2 ± 0.3
GeoB 12811	12.57	26.02	2980	30.1	4.3 ± 1.4
GeoB 12815	10.00	27.23	4672	47.1	0.1 ± 0.1

[a] The mean and one standard error were calculated based on determined TOC values at a depth resolution of roughly every 1 m.

with a heated bed of mercuric oxide to form mercury vapor that was subsequently detected in a photometer cell. The instrument was operated at a column oven temperature of 105 °C and a bed temperature of 265 °C with N_2 (purity = 99.999%) as carrier gas. The instrument was calibrated with a 10 ppm H_2 primary standard (Air Liquide, Germany) on a daily basis. For sample injection, we did not use the syringe port provided by the supplier but the injection valve, since puncturing of the syringe port by the needle introduces atmospheric H_2 into the system. Typically, more than 3 mL of gas sample was injected to thoroughly flush the 1-mL sample loop for the extraction approach, and 1 mL of gas sample was required to flush the 100-μL sample loop for the headspace equilibration technique. The instrumental LoD, calculated as three times the standard error of multiple measurements of 100 ppb H_2 diluted from the primary standard, was about 34 ppb or 1.4 pmol for the 1 mL loop. Ultrapure N_2 gas (the bypass gas out of the Peak Performer 1) was used to dilute the gas standard.

$[H_2]_{INC}$. For the determination of dissolved H_2 concentrations in incubated samples, we followed the headspace equilibration protocol published in Hoehler et al. (1998). In brief, a sediment sample of 2–3 mL was extruded into a 22-mL headspace vial, immediately sealed with a thick black butyl stopper (Glasgerätebau Ochs GmbH, Bovenden, Germany; boiled once with 0.1 N NaOH and twice with Milli-Q before use), crimp capped, and flushed with N_2 (purity = 99.999%) for at least 1 min. Samples were incubated right after core retrieval in the dark at the in situ temperature of 4 °C and H_2 concentrations in the headspace gas were analyzed every 1–3 days. Aiming to reach steady-state conditions, all shipboard incubations were continued as long as possible (2–25 days). In order to avoid a drop of gas pressure in the headspace due to sampling, 1 mL of ultrapure N_2 was injected into the headspace immediately after each analysis.

$[H_2]_{EXT}$. For direct determination of dissolved H_2, we used an extraction method resembling the recently published protocol by D'Hondt et al. (2009). A sediment sample of 2–3 mL was extruded into a 22-mL headspace vial, which was immediately filled with a solution to the top, sealed with a thin gray chlorobutyl stopper (VWR International, LLC), and crimp capped. The choice of solution and its preparation were investigated in the present study (see below). The sampling and preparation steps typically took less than 1 min to minimize diffusive loss of gas. In the vial, a headspace was created by displacing 5–7 mL of the aqueous phase with an equal volume of ultrapure N_2 gas. Once the headspace reached the intended volume, the gas-in needle was removed first, and the overpressure in the vial was allowed to escape through the liquid-out needle. The expelled liquid was collected in a syringe and the volume, which corresponds to the generated headspace, was recorded. The vial was then mixed using a vortex mixer, turned upside down and allowed to sit for 20 min to let H_2 diffuse out of the interstitial water and equilibrate with the headspace. For H_2 analysis, the headspace gas was displaced into a N_2-flushed plastic syringe by injecting into the vial the same solution used to prepare sediment slurries. Care was taken not to evacuate the headspace during the gas sampling step; otherwise, atmospheric H_2 could be drawn into the vial through the stopper, leading to erroneously high H_2 signals.

CH_4. Concentrations of dissolved methane were determined according to previously reported protocols (Kvenvolden and McDonald, 1986; D'Hondt et al., 2003): 2–3 mL of wet sediment were enclosed in a gas-tight 22-mL glass vial and heated for 30 min at 60 °C before 100–200 μL gas samples were taken from the headspace with gas-tight syringes and analyzed immediately by gas chromatography-flame ionization detector (GC-FID). The GC-FID was calibrated on a daily basis using a hydrocarbon gas standard (Scotty). Based on the partial pressure of methane in the headspace gas and the headspace volume, the total amount of released methane was quantified and normalized to the pore-water volume of the extracted sediment sample, using the sample volume and corresponding porosity data of the solid phase sample.

2.3.2. Pore-water analysis

Methods for determining ionic species have been described elsewhere (Goldhammer et al., 2011) and are briefly summarized below. Immediately after pore waters had been sampled by rhizons on board RV *Meteor*, ferrous iron (Fe^{2+}) was measured photometrically (Hach Lange DR 5000 photometer) with a LoD of 0.2 μmol L^{-1}. An iron sensitive color complex was formed by adding 1 mL of sample to 20 μL of Ferrospectral solution (Merck) in polystyrene cuvettes, and the extinction was measured at a wavelength of 565 nm. Samples with high Fe^{2+} concentrations were diluted with oxygen-free H_2O to match the calibration range. Dissolved ammonium (NH_4^+) was quantified with the flow injection/gas separation technique after Hall and Aller (1992), pH values were determined using a pH electrode (Hamilton Double Pore), and samples were preserved and stored at +4 °C and −20°C for shore-based inorganic and organic analyses, respectively. Dissolved

hydrogen sulfide (HS^-) was determined on sample splits fixed with zinc acetate using the photometric methylene blue method (Cline, 1969). Dissolved anions (chloride, Cl^-; bromide, Br^-; SO_4^{2-}) were determined by ion chromatography (Metrohm 861 Advanced Compact IC, column A Supp 5, conductivity detection after chemical suppression). Dissolved cations (sodium, Na^+; magnesium, Mg^{2+}; calcium, Ca^{2+}; potassium, K^+) were measured in acidified samples by inductively coupled plasma optical emission spectrometry (Perkin Elmer Optima 3300R). DIC, mostly in the form of bicarbonate (HCO_3^-) at neutral pH, was quantified as CO_2 after acidification and purging by non-dispersive infrared spectrometry (Shimadzu TOC-V) in sample splits fixed with zinc acetate. At Site GeoB 12802, concentrations of volatile fatty acids were analyzed by isotope-ratio-monitoring liquid chromatography/mass spectrometry (ThermoFinnigan) as described previously (Heuer et al., 2006, 2009).

2.3.3. Solid phase analysis

TOC contents were measured on freeze-dried, homogenized, decalcified (6 N HCl), and dried samples using a Leco CS 200 at the University of Bremen. Porosity was determined by weight difference, before and after freeze drying the wet sediment sample and is expressed as a volume ratio (volume of pore water/volume of bulk sediment) assuming a pore-water density of 1.024 g cm^{-3} (Blum, 1997).

2.4. Calculations

2.4.1. Hydrogen concentrations

The incubation and the extraction methods require different approaches to deduce the concentration of dissolved H_2 from the analysis of H_2 in headspace gas, but for both methods the first step is to convert H_2 concentrations in the headspace from mole fractions (χ_{H_2}, expressed as ppb, obtained from chromatographic analysis) to molar concentrations ($[H_2]_g$, expressed as nmol L^{-1}):

$$[H_2]_g = \chi_{H_2} \times P \times R^{-1} \times T^{-1} \quad (1)$$

where P is the total gas pressure in the headspace (1 atm), R is the universal gas constant, and T is the temperature in kelvin. At equilibrium, the corresponding concentration of dissolved H_2 ($[H_2]_{aq}$) is:

$$[H_2]_{aq} = \beta \times [H_2]_g \quad (2)$$

where β is an experimentally determined solubility constant corrected for temperature and salinity (Crozier and Yamamoto, 1974).

For the headspace equilibration technique, the concentration of H_2 dissolved in interstitial water ($[H_2]_{INC}$, expressed as nmol L^{-1}) is assumed to be in equilibrium with the gas phase and calculated as:

$$[H_2]_{INC} = \beta \times [H_2]_g \quad (3)$$

For the extraction approach, the concentration of H_2 dissolved in interstitial water ($[H_2]_{EXT}$, expressed as nmol L^{-1}) is determined via mass balance:

$$[H_2]_{EXT} = ([H_2]_g \times V_g + [H_2]_{aq} \times V_{aq}) \times V_{sed}^{-1} \times \phi^{-1} \quad (4)$$

where V_g represents the volume of the headspace and V_{aq} the volume of the aqueous phase, including the pore water and the solution added. V_{sed} is the volume of the sediment sample, and ϕ is the sediment porosity. $[H_2]_g$ and $[H_2]_{aq}$ are obtained from Eqs. (1) and (2), respectively. The β value is 0.0174 for water and 0.0150 for 3.5% NaCl solution at 25 °C (Crozier and Yamamoto, 1974). In the case in which saturated NaCl solution (salinity = 35%) was used, the β value corrected for the "salting-out effect" was estimated by the Sechenov equation with the Sechenov constant calculated by the empirical model described in Weisenberger and Schumpe (1996). We obtained a β value of 0.00423 for H_2 in saturated NaCl at 25 °C.

2.4.2. Thermodynamic calculations

The thermodynamic calculation had the objective of determining the H_2 concentration for a metabolic reaction under the critical ΔG value, with the following steps: first, the $\Delta G°$ of a reaction under in situ conditions was calculated using the software package SUPCRT92 (Johnson et al., 1992) and the thermodynamic data of dissolved species from Shock and Helgeson (1990) (Table 3). Second, we computed the activities of SO_4^{2-}, HS^- and HCO_3^- by use of PHREEQC software (Parkhurst and Appelo, 1999) with

Table 3
Thermodynamic parameters of reactions discussed in this study. Only the standard Gibbs free energies based on the state condition of GeoB 12802 ($T = 4$ °C, $P = 8.1$ MPa) are listed.

Reaction	$\Delta G°$ (kJ mol^{-1} reaction)
Iron (iron(III) oxide-hydroxide) reduction $2FeO(OH) + 4H^+ + H_{2,aq} \rightarrow 2Fe^{2+} + 4H_2O$	−308
Sulfate reduction $SO_4^{2-} + H^+ + 4H_{2,aq} \rightarrow HS^- + 4H_2O$	−261
Methanogenesis $HCO_3^- + H^+ + 4H_{2,aq} \rightarrow CH_{4,aq} + 3H_2O$	−231
Butyrate fermentation $CH_3CH_2CH_2COO^- + 3H_2O \rightarrow CH_3CH_2COO^- + HCO_3^- + 3H_{2,aq} + H^+$	+170
Propionate fermentation $CH_3CH_2COO^- + 3H_2O \rightarrow CH_3COO^- + HCO_3^- + 3H_{2,aq} + H^+$	+173
Acetogenic CO_2-reduction $2HCO_3^- + H^+ + 4H_{2,aq} \rightarrow CH_3COO^- + 4H_2O$	−216

the input of the measured concentrations of major ions (Na^+, Mg^{2+}, Ca^{2+}, K^+, NH_4^+, Cl^-, Br^-, SO_4^{2-}, HS^-, HCO_3^-). Finally, assuming the critical ΔG required to sustain life is -15 kJ per mol reaction (Schink and Stams, 2006) we calculated the corresponding H_2 activities by recasting the equation

$$\Delta G = \Delta G^{\circ} + RT \ln Q \quad (5)$$

and solving for the H_2 term in Q, which is the activity quotient of the reactants and products.

3. RESULTS AND DISCUSSION

3.1. Evaluation and optimization of the extraction method for H_2 analysis

3.1.1. Background H_2, blanks, and methodological limit of detection

The presence of background H_2 in the laboratory is a major challenge for sensitive and reliable analysis of low concentrations of dissolved H_2 by the extraction method. During the analytical procedure, H_2 can be introduced into the sample from various sources including the solution used for sample extraction, the ultrapure N_2 gas used for the creation of the container headspace, and ambient laboratory air. Moreover, additional H_2 might be formed during the extraction of sediment and add to the background.

The presence of background H_2 causes high analytical blanks and results in a high LoD. While we use the term background H_2 to express the actual concentration of H_2 in various H_2 sources in the laboratory (solution, air, gas), we use the term blank to describe the H_2 concentration that the background would account for in a representative sample. For determination of blanks the extraction method is conducted without sample, and the released amount of H_2 is detected and divided by a pore-water volume representative of real samples. The magnitude and reproducibility of the blank finally determine the methodological LoD (LoD_m), which denotes a statistically significant sample signal that can be obtained by the extraction method and is distinct from the much lower instrumental LoD (cf. Section 2.3.1). We followed the conventional definition of $LoD = \mu_B + 3 \times s_B$, where μ_B and s_B are the mean and standard error of replicate blank measurements, to calculate the LoD_m.

3.1.2. Background H_2 in solutions used for extraction

The initial step of the extraction method is to completely fill the sample containing headspace vial with solution. An ideal solution would not only be free of background H_2 but also stop or retard microbial reactions in the sediment so that the concern of headspace-induced H_2 production can be minimized. We tested deionized water that is similar to the distilled water used by D'Hondt et al. (2009), 3.5% NaCl solution which represents the salinity of seawater, and saturated 35% NaCl solution which has a salting-out effect and should inhibit biological activity in normal marine sediments where the microbial groups are presumably adapted to seawater salinity. We did not use additional inhibitors of microbial activity, such as formaldehyde and alkali, since they are known to create artificially high H_2 concentrations (Krämer and Conrad, 1993).

If open to the laboratory environment, the solution will equilibrate with atmospheric H_2. At equilibrium, the atmospheric H_2 partial pressure of 530 ppb (Novelli et al., 1999) corresponds to dissolved H_2 concentrations ($[H_2]_{aq}$) of 0.4, 0.3, and 0.1 nmol L^{-1} in deionized water, 3.5% NaCl and 35% NaCl, respectively (Eqs. (1) and (2)). We found that the H_2 background of the freshly prepared solutions (i.e., deionized water from the laboratory tap and NaCl crystals dissolved in water in a glass bottle) was 5–45 times higher than the expected equilibrium concentrations (Table 4). The background was particularly high in saturated NaCl solution where it reached 4.4 ± 0.6 nmol L^{-1}. When the solutions were stored in an open beaker and allowed to equilibrate with the atmosphere for >5 h, levels of background H_2 decreased but did not reach equilibrium concentrations. In saturated NaCl solution the H_2 background declined to 50% of its initial value (Table 4). Additional bubbling of the solutions with N_2 for 20 min further reduced the variation of H_2 background in both the 3.5% NaCl and 35% NaCl solution but showed no positive effect in the case of deionized water. The levels of background H_2 in N_2-bubbled salty solutions and deionized water were similar within the precision of the method. Stirring of the solutions for 3 h helped to decrease the variation of H_2 background in saturated NaCl solution, but showed little effect in the case of deionized water and 3.5% NaCl solution. For the shipboard processing of samples, the solutions are stored for 20–30 min in 50 mL plastic syringes with their Luer tips fitted with a two-way plastic valve. This treatment did not change the H_2 background: concentrations of dissolved H_2 were 0.8 ± 0.4 nmol L^{-1} in deionized water, 1.5 ± 0.6 nmol L^{-1} in 3.5% NaCl solution, and 1.6 ± 0.5 nmol L^{-1} in saturated NaCl solution.

Independent of salt content and treatment, the H_2 background was always higher than the theoretical concentrations of dissolved H_2 in equilibrium with the atmosphere. These observations suggest that the H_2 background is not solely driven by equilibration of the solution with the atmosphere. Instead, they point to the introduction of significant amounts of additional background H_2 from other unconstrained sources during the analytical procedure.

3.1.3. Background H_2 in the container headspace

The second step of the extraction method is the creation of an artificial headspace in the completely filled, sealed vial by replacement of about one third of the solution with ultrapure N_2. Regular tests of the ultrapure N_2 in the framework of this study confirmed that the gas does not carry any detectable H_2 background. However, atmospheric H_2 can potentially enter the headspace via permeation of H_2 through the container or via seepage of H_2 through the chlorobutyl rubber stopper. The permeability constant of H_2 through the most common soda-lime glass is 2.5×10^{-5} pmol cm cm^{-2} min^{-1} atm^{-1} at 25 °C based on the parameters and the equation provided by Souers et al. (1978). According to the general gas permeability equation (Crank, 1975; Table 5), the amount of H_2 entering

Table 4
Background H_2 concentrations (nmol L^{-1}) in deionized water, 3.5% NaCl and 35% NaCl after different treatments.

Treatment	Deionized water	3.5% NaCl	35% NaCl
a. Calculated $[H_2]_{aq}$ when the solution is equilibrated with H_2 in the atmosphere (530 ppb)[a]	0.4	0.3	0.1
b. Freshly prepared solution, without bubbling	1.9 ± 1.2	1.4 ± 0.7	4.4 ± 0.6
c. Equilibrated with the atmosphere for >5 h	1.5 ± 1.1	1.5 ± 0.6	2.3 ± 1.6
d. Equilibrated with the atmosphere for >5 h + bubbled with N_2 for >20 min	2.0 ± 1.4	0.8 ± 0.1	1.2 ± 0.9
e. Stirred for 3 h	1.6 ± 1.2	1.7 ± 0.8	0.7 ± 0.1

[a] The global average H_2 concentration in the atmosphere is from Novelli et al. (1999). The $[H_2]_{aq}$ was calculated using the Bunsen constants (Crozier and Yamamoto, 1974) for deionized water and 3.5% NaCl. The salting-out effect of 35% NaCl was estimated using the procedure described in Weisenberger and Schumpe (1996).

the container through its glass wall within a permeation time of 20 min would cause a negligible solution background of only 2.7×10^{-9} nmol L^{-1}. Similarly, the permeability of chlorobutyl rubber for H_2 is low (5.2×10^{-2} pmol cm cm^{-2} min^{-1} atm^{-1} at 20 °C; Pauly, 1989) and the amount of atmospheric H_2 permeated through chlorobutyl rubber stoppers is negligible for a period of 20 min.

However, the stoppers get punctured by needles when the headspace is created and when gas samples are withdrawn. The punctures might provide a passage for the introduction of atmospheric H_2. We tested the impact of needle punctures on the H_2 background using a set of empty 11 mL headspace vials that were sealed with chlorobutyl rubber stoppers and crimp capped. All stoppers were punctured by gauge 23 or 26 needles at the beginning of the experiment when the vials were evacuated and flushed three times with ultrapure N_2 and at the end when deionized water was injected to push out headspace gas for H_2 analysis. In two series of vials the stoppers were additionally punctured twice by a pair of gauge 23 and 26 needles connected to N_2-flushed syringes, in one case before and in the other one after the vials were allowed to sit for 20 min with their tops immersed in water, while no further needle punctures were added in a third series which served as control. In vials with additional needle punctures H_2 concentrations were distinctly higher than in the control (Table 5) and the H_2 background in the headspace increased strongly even when addition of extra punctures was immediately followed by analysis, suggesting that seepage takes place at the time when a septum is punctured. H_2 concentrations in the headspace gas ranged from 22 to 259 ppb and correspond to background concentrations of 0.4–4.1 nmol L^{-1} when normalized to an extraction solution with a volume of 15 mL (Table 5).

In summary, the seepage of small amounts of H_2-rich (530 ppb) ambient air into the headspace via needle punctures in the course of sampling is a remarkable source of background H_2 and provides an explanation why the analyzed background H_2 in extraction solutions always exceeded the theoretical concentrations of dissolved H_2 in equilibrium with atmospheric H_2 (Table 4).

3.1.4. Background H_2 formed during extraction of sediments

In active systems where the residence time of H_2 is short relative to the equilibration period, the extraction of H_2 into the headspace volume might stimulate H_2 production in the slurry and thus yield erroneously high H_2 concentrations. Therefore, we tested the extraction method with deionized water and both 3.5% and 35% NaCl solution using a sample of shallow tidal flat sediment from the North Sea with a sulfate-reducing redox regime. The sediment was chosen because it was expected to provide low initial concentrations of pore-water H_2 in the presence of high microbial H_2 turnover. The 3.5% NaCl solution represents the salinity of seawater. It is unlikely to inhibit the metabolism of marine microorganisms and likely to reveal excess hydrogen production in the selected active surface sediment. In contrast, deionized water and saturated NaCl solution were expected to inhibit biological activity and headspace-induced excess H_2 production since they exert extreme osmotic pressure which slows down or stops the activity of cells, as is often observed in the Na^+ concentration gradient tests performed on new marine isolates (e.g., Sowers and Ferry, 1983).

Extraction of the sediment sample with different solutions yielded distinctly different results. Background-corrected H_2 concentrations reached 16.8 ± 3.9 nmol L^{-1} in 3.5% NaCl, but only 4.6 ± 1.9 nmol L^{-1} and 4.1 ± 3.1 nmol L^{-1} in deionized water and 35% NaCl, respectively. The results reveal considerable excess H_2 production when active anoxic sediment is treated with 3.5% NaCl solution and the suppressive effect of deionized water and saturated NaCl solution on this process.

3.1.5. Test of the optimized method

In the optimized extraction method, 35% NaCl solution was freshly prepared, bubbled with N_2 or stirred in an open beaker for at least 3 h to allow equilibration with the atmosphere, and stored in plastic syringes during core processing for less than 30 min. With this procedure, the measured average background H_2 was 1.6 ± 0.5 nmol L^{-1}, equivalent to 25.6 ± 8.2 pmol H_2 per sample vial (a 22 mL vial with 16 ± 1 mL solution). In our field study offshore of Namibia, the volume and porosity of sediment taken for H_2 extraction were on average 2.8 mL and 0.7, respectively, with a corresponding pore-water volume of 2.0 mL. Normalization of background H_2 to the average pore-water volume of samples and error propagation result in a H_2 blank of 13.1 ± 4.2 nmol L^{-1}. The corresponding LoD_m is 25.5 nmol L^{-1}. Though the highly reproducible blank values ensure a more consistent LoD_m compared to previous

Table 5
Contamination of the container headspace by atmospheric H_2.

Calculation or treatment	H_2 in headspace (ppb)	Corresponding dissolved $[H_2]$ in solution (nmol L^{-1})
Permeation of atmospheric H_2 into the container headspace[a]	3.6×10^{-8}	2.3×10^{-9}
Leakage of atmospheric H_2 into the container headspace[b]		
a. Control, wait 20 min	22–33	0.4–0.5
b. Puncture the septum with needles of gauge 23 and 26, twice of each, wait 20 min	58–259	0.9–4.1
c. Wait 20 min, puncture the septum with needles of gauge 23 and 26, twice of each	50–183	0.8–2.9

[a] Calculation of the total amount of permeated H_2: We used the recast gas permeability equation $n = \Phi \times A \times t \times \Delta P \times d^{-1}$, where n is the amount of gas molecules, Φ is the permeability constant, A is the contact area between the solid and the gas, t is the length of the permeation time, ΔP is the difference in partial pressure of the gas between both sides of the solid, and d is the thickness of the solid. For the 22 mL headspace vial used in the study, the wall thickness is 0.11 cm, and the contact area to air for a 6 mL headspace is 15 cm^2. The permeation time is 20 min. A solution volume of 16 mL was used to calculate the corresponding dissolved H_2 concentration.

[b] Calculation of the corresponding dissolved H_2 concentration: The H_2 leakage was assumed to be independent from the volumes of the gaseous phase. Therefore, the amount of H_2 detected in the 11-mL headspace vials was divided with an aqueous phase volume of 16 ± 1 mL (22 mL headspace vial with a 6 ± 1 mL headspace) to acquire the corresponding dissolved H_2 concentrations.

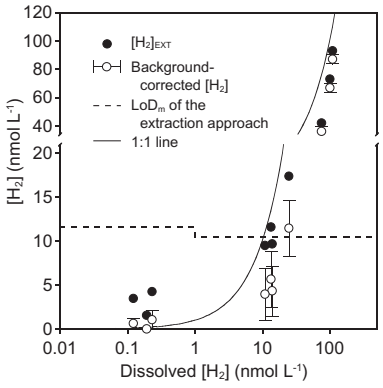

Fig. 2. Extraction of sediment samples with known dissolved $[H_2]$. Selected sediment samples having distinct ranges of dissolved $[H_2]$, inferred from the final $[H_2]_{INC}$ after prolonged incubation (36–42 days), were extracted for H_2 analysis using the protocol optimized in this study. The methodological limit of detection (LoD_m) varied among different sets of samples due to varied volumes of sediment samples and glass containers. Variation in the background H_2 ($\pm$two standard errors) resulted in the error bars of the background-corrected $[H_2]$.

studies (D'Hondt et al., 2009), further improvements are required before the in situ consumption of H_2 by energetically more favorable processes than methanogenesis and acetogenesis can be investigated reliably by the extraction method. Most importantly, the direct introduction of gaseous, atmospheric H_2 into the sample vials in the course of sampling needs to be minimized in order to reduce the background. With the current method, a combination of larger sediment volumes and smaller sampling vials (thereby less extraction solution) can help to lower the blank.

In order to further validate our extraction method, we analyzed $[H_2]_{EXT}$ in sediment samples in which we had previously monitored concentrations of dissolved H_2 by the incubation method. The selected three groups of samples have distinct ranges of dissolved H_2: GeoB 12803, 0.12–0.23 nmol L^{-1}; GeoB 15105, 11.1–14.1 nmol L^{-1}; GeoB 15101 and 15102, 25–110 nmol L^{-1}. The samples were immediately extracted after incubation (36–42 days) was finished and the results are presented in Fig. 2. Note that the LoD_m here (~11 nmol L^{-1}) is lower from that for our field survey due to larger sediment volumes or smaller glass containers used in this experiment.

For the samples in which dissolved H_2 was lower than the LoD_m of the extraction method, the $[H_2]_{EXT}$ values are lower than the LoD_m. The background-corrected H_2 concentrations range from negative (plotted to zero in Fig. 2) to slightly positive values and are not precise enough to represent the low dissolved H_2 concentrations. In contrast, for samples with elevated levels of dissolved H_2, we obtained significant $[H_2]_{EXT}$ values. The background-corrected H_2 concentrations underestimate the dissolved H_2 concentrations, pointing to the loss of H_2 during the sampling and extraction procedure. These results demonstrate that $[H_2]_{EXT}$ values above the LoD_m can be considered conservative estimates of sedimentary H_2 concentrations.

3.2. Study of the sediment transect off Namibia

3.2.1. Geochemical environments and prediction of $[H_2]_{TD}$

Along a transect of sites across the continental margin off Namibia, TOC contents decline (Table 2) and the distribution of redox zones changes distinctly with increasing water depth (Fig. 3). At the shallowest station GeoB 12802, pore-water profiles of Fe^{2+}, SO_4^{2-} and methane indicate intensive anaerobic degradation of organic matter along with a succession of iron reduction (core top to 10 cm below seafloor, referred to as cmbsf hereafter), sulfate reduction (10–260 cmbsf) and methanogenesis (>260 cmbsf) in the upper 6 m of sediment. Where acetate concentrations were high enough ($\geqslant$10 μmol L^{-1}) stable carbon isotope analyses did not reveal a significant contribution of acetogenic CO_2 reduction to the pore-water acetate pool. $\delta^{13}C$ values of acetate are −21.1‰ at 149 cmbsf and average -25.4 ± 1.1‰ in the interval of 415–440 cmbsf.

Iron reduction (2–20 cmbsf) and sulfate reduction (>20 cmbsf) are also observed at Site GeoB 12803 in ~2000 m water depth with profiles of Fe^{2+} and SO_4^{2-} suggesting lower rates of organic matter mineralization than at Site GeoB 12802. Methane concentrations rise rapidly with depths >400 cmbsf, but the coexisting high SO_4^{2-}

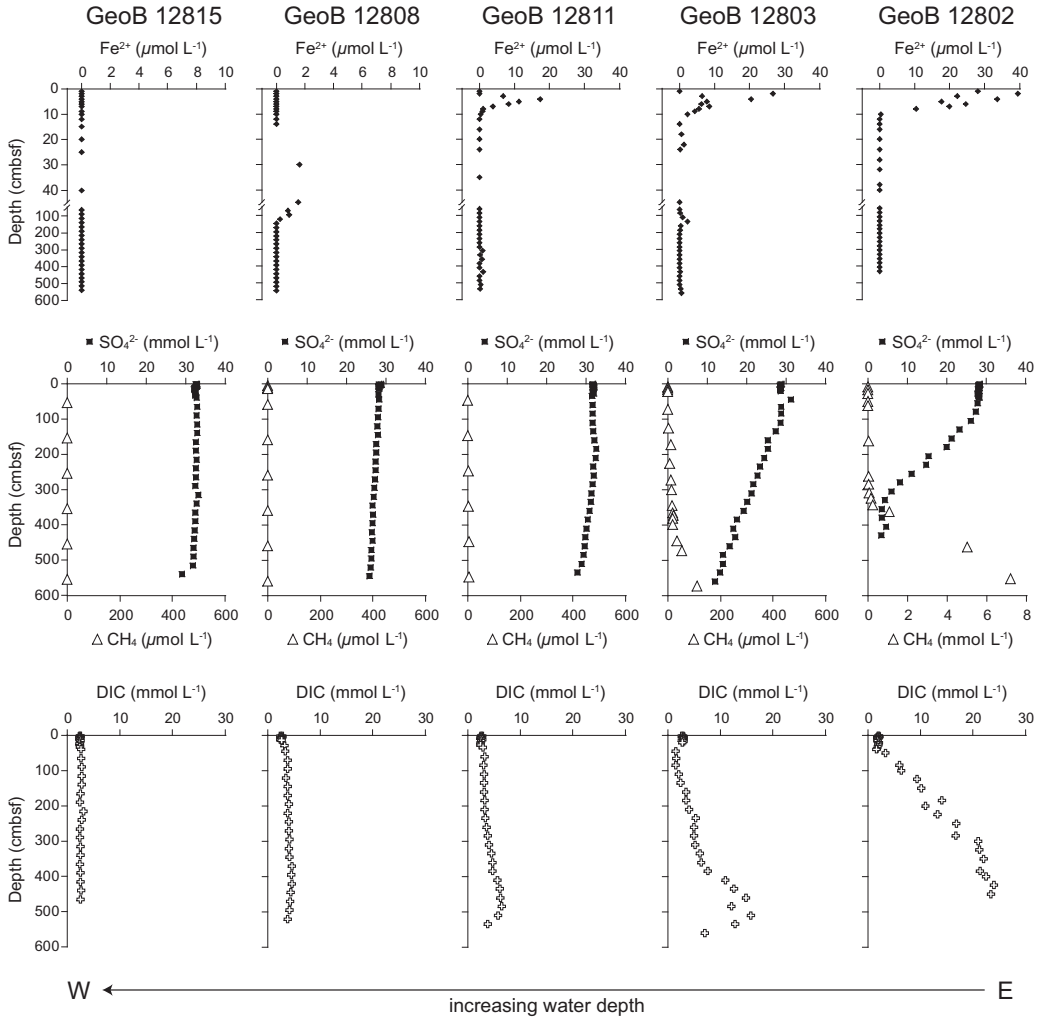

Fig. 3. Depth profiles of Fe^{2+}, SO_4^{2-}, methane and dissolved inorganic carbon (DIC) concentrations in sediment interstitial waters at five stations, offshore Namibia. Note the difference in scale for methane concentrations at Site GeoB 12802.

concentrations (12–17 mmol L^{-1}) suggest that methanogenesis is not the major mode of terminal metabolism (cf. Martens and Berner, 1974). At Site GeoB 12811 (~3000 m water depth), iron reduction (3–10 cmbsf) and sulfate reduction (>10 cmbsf) are still observed; the importance of these processes ceases at Sites GeoB 12808 and GeoB 12815 in ~4000 m and ~4500 m water depth, respectively, where pore-water Fe^{2+} is approaching the LoD and SO_4^{2-} concentrations remain close to seawater values throughout the sampled sediment layer. Pore-water methane is below the LoD in the upper 6 m of the latter three sites.

The decreasing intensity of organic matter remineralization is also reflected in the pore-water profiles of DIC (Fig. 3). While DIC concentrations increase strongly with sediment depth from ca. 2.5 mmol L^{-1} to 24 mmol L^{-1} and 15 mmol L^{-1} at the relatively shallow Sites GeoB 12802 and GeoB 12803, respectively, a maximal concentration of only 6.5 mmol L^{-1} is reached at the deeper Site GeoB 12811. At the two deepest stations GeoB 12808 and 12815, DIC concentrations show low, constant values of 4 mmol L^{-1}. The measured pH from the five sites has an average value of 7.6 (±0.1). The estimated bottom water temperatures at all stations were 2–4 °C.

The variations in pore-water chemistry and in situ pressure along the transect of sites impact the ΔG values of H_2-consuming reactions. Based on thermodynamic considerations (cf. Section 2.3.2), we calculated the downcore distribution of $[H_2]_{TD}$ for iron reduction, sulfate reduction, methanogenesis, and acetogenic CO_2-reduction, with an example of Site GeoB 12802 shown in Fig. 4. At this station, we expect threshold concentrations of 10^{-9}–10^{-14} nmol L^{-1} H_2 for iron reduction, 0.01–0.3 nmol L^{-1} H_2 for sulfate reduction, 0.7–4.2 nmol L^{-1} H_2 for methanogenesis and 8–39 nmol L^{-1} H_2 for acetogenic CO_2-reduction. Compared with the expected $[H_2]_{TD}$ values reported for surface sediments (Table 1), the threshold concentrations in the deep-water sediments off Namibia are lower by 1–12 orders of magnitude.

3.2.2. $[H_2]_{INC}$ – H_2 in shipboard incubation of sediment

During shipboard incubation, some samples reached an apparent steady state after 10 days of incubation but others

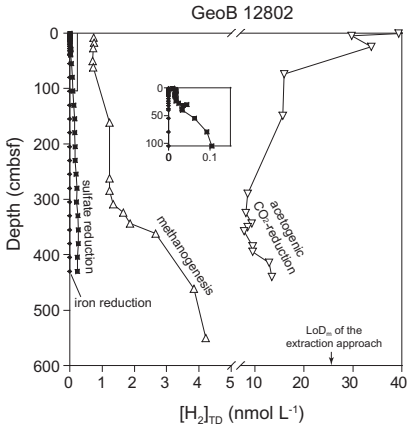

Fig. 4. Downcore distribution of $[H_2]_{TD}$ values for iron reduction, sulfate reduction, methanogenesis, and acetogenic CO_2-reduction at GeoB 12802. See text for details of thermodynamic calculation. The enlarged insert shows the $[H_2]_{TD}$ values for iron reduction and sulfate reduction in the upper sediment column. The methodological limit of detection (LoD_m) of the extraction approach optimized in this study is also marked. The range of H_2 concentrations at which a given mode of terminal metabolism maintains its superiority is controlled thermodynamically by this particular reaction and its next most favorable process.

not, even when the maximal incubation duration was allowed (25 days). In the latter case, we averaged the second last two measurements to obtain a $[H_2]_{INC}$ value. For samples from Sites GeoB 12811 and GeoB 12815 the time schedule of the cruise only allowed incubation for 5 and 2 days, respectively, and the resulting data need to be interpreted with caution.

At the shallow Site GeoB 12802 (Fig. 5), which shows the highest TOC contents, strongest remineralization and closest succession of redox zones within the transect, $[H_2]_{INC}$ remains below the thermodynamically predicted threshold concentrations $[H_2]_{TD}$ in the methanogenic zone but exceeds them in the sulfate reduction zone and in the near-surface sediment where high Fe^{2+} concentrations suggest active iron reduction (Fig. 3). An exceptionally high $[H_2]_{INC}$ value of 14.6 nmol L^{-1}, which is above the threshold for acetogenic CO_2-reduction (Fig. 4), was observed at 260 cmbsf, close to the upper SMTZ.

At Site GeoB 12803 (~2000 m water depth), where TOC contents are lower and remineralization less intensive than at Site GeoB 12802, $[H_2]_{INC}$ exceeds $[H_2]_{TD}$ throughout the upper 6 m of the sediment, except for a distinct minimum of $[H_2]_{INC}$ at 382 cmbsf. In the iron reduction zone (2–20 cmbsf), $[H_2]_{INC}$ exceeds the $[H_2]_{TD}$ for iron reduction by three orders of magnitude. In the sulfate reduction zone,

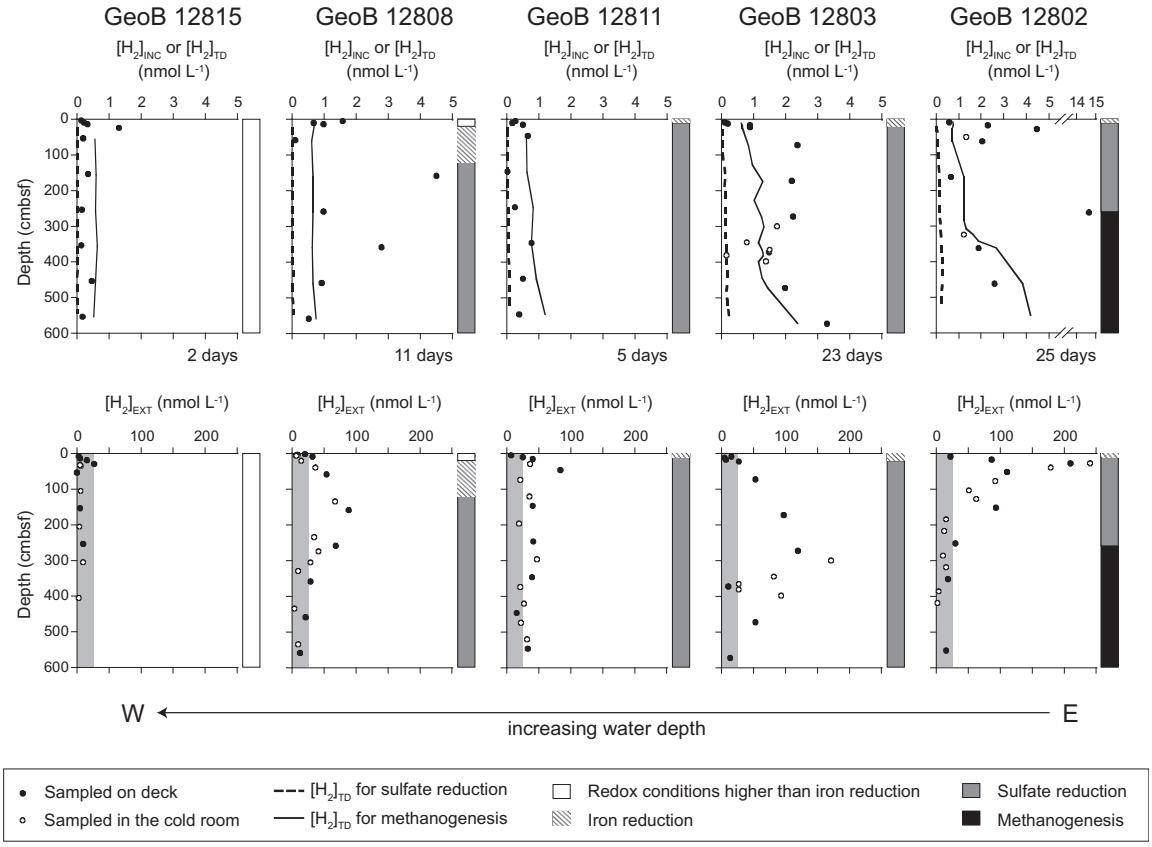

Fig. 5. Depth profiles of $[H_2]_{INC}$ and $[H_2]_{EXT}$ in sediment interstitial waters at five stations, offshore Namibia. The distribution of $[H_2]_{TD}$ for sulfate reduction and methanogenesis is also plotted for comparison. The duration of sediment incubation was listed for individual stations. The shaded areas mark the methodological limit of detection of the extraction approach.

$[H_2]_{INC}$ concentrations are 2- to 60-fold higher than the $[H_2]_{TD}$ for both sulfate reduction and methanogenesis. This trend continues toward the bottom of the core where the methane level is slightly elevated in the presence of roughly 10 mmol L^{-1} sulfate. The distinct minimum of $[H_2]_{INC}$ at 382 cmbsf coincides with the shallowest depth where porewater methane is detectable. The underlying reasons for this subsurface minimum remain elusive; visual core description does not reveal any striking differences between this layer and the adjacent sediment layers.

High $[H_2]_{INC}$ values of up to 4 nmol L^{-1} are found at the deep Site GeoB 12808 (~4000 m water depth) where iron reduction, sulfate reduction or methanogenesis are not active in the low-TOC sediment, and the uniformly low DIC concentrations indicate low rates of organic matter remineralization. Similar to the TOC-rich Site GeoB 12803, the $[H_2]_{INC}$ values are higher than the $[H_2]_{TD}$ values for iron reduction, sulfate reduction and, except for one case (58 cmbsf), also for methanogenesis at Site GeoB 12808. Likewise, $[H_2]_{INC}$ in sediments from Sites GeoB 12811 (~3000 m water depth) and 12815 (~4500 m water depth) exceeds $[H_2]_{TD}$ for sulfate reduction.

3.2.3. $[H_2]_{EXT}$ – H_2 extracted from sediment

Our thermodynamic calculations suggest that close syntrophic relationships between H_2-producing and -consuming microorganisms would draw H_2 concentrations below the LoD_m of our extraction method, but, 55% of the $[H_2]_{EXT}$ data presented in the profiles are above the LoD_m (26 nmol L^{-1}) (Fig. 5). Except for the deepest site GeoB 12815, the other four sites have the following features in common: the $[H_2]_{EXT}$ values are usually below or close to the LoD_m in the near-surface sediments, reach a subsurface maximum of 80–240 nmol L^{-1}, and decrease with depth to below or around the LoD_m. A similar downcore distribution of $[H_2]_{EXT}$ with maximum values of up to 60 nmol L^{-1} has been reported by Novelli et al. (1987). Along our transect, maximum values of $[H_2]_{EXT}$ decline with decreasing TOC contents, but the depths of the subsurface maxima appear to be independent of water depth and TOC content. Moreover, vertical distributions of $[H_2]_{EXT}$ show no obvious relationship to profiles of Fe^{2+}, SO_4^{2-}, methane and DIC (Fig. 5). The absence of above-LoD_m $[H_2]_{EXT}$ in all but one sample from organic-lean sediments at Site GeoB 12815 agrees with previous findings (Table 1; Novelli et al., 1987; D'Hondt et al., 2009).

In general, the direct extraction of H_2 from pore waters resulted in distinctly higher H_2 concentrations than the incubation of sediments in the laboratory. Above-LoD_m values of $[H_2]_{EXT}$ exceed the corresponding $[H_2]_{INC}$ values by one to two orders of magnitude. Though a strong correlation between $[H_2]_{INC}$ and $[H_2]_{EXT}$ data is lacking (the R^2 value of least squares linear regression between both datasets is <0.4), their profile shapes share the following features (Fig. 5): (1) both $[H_2]_{INC}$ and $[H_2]_{EXT}$ values are low in the uppermost sediments, (2) the subsurface maxima observed in some $[H_2]_{EXT}$ profiles (e.g., GeoB 12802 and 12808) coincide with the highest $[H_2]_{INC}$ value, and (3) the conspicuous subsurface $[H_2]_{INC}$ minimum detected at 382 cmbsf at Site GeoB 12803 is also well delineated in $[H_2]_{EXT}$.

3.2.4. Comparison of $[H_2]_{INC}$ and $[H_2]_{EXT}$

To systematically compare $[H_2]_{INC}$ and $[H_2]_{EXT}$ and to extract information pertaining to syntrophic coupling, we combined both datasets in Fig. 6 based on the following considerations:

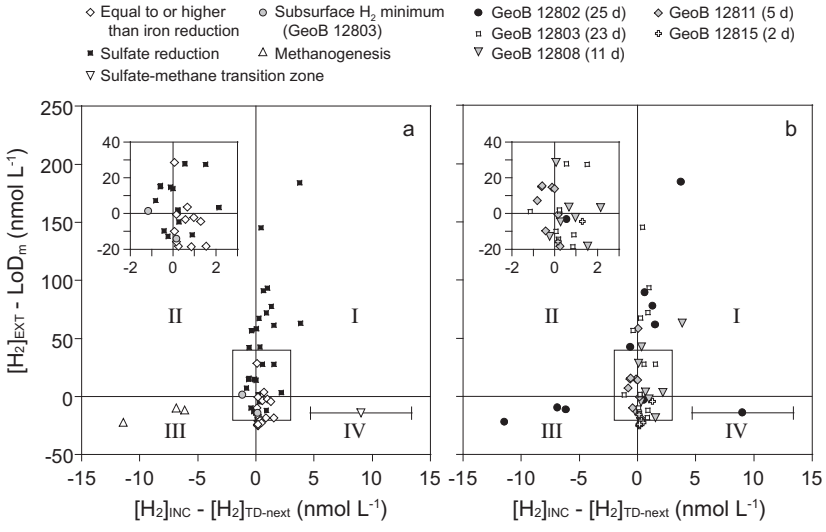

Fig. 6. Distribution of $[H_2]_{INC}$–$[H_2]_{TD\text{-}next}$ versus $[H_2]_{EXT}$–LoD_m, categorized based on either (a) redox regime or (b) incubation duration; each with separate legends. Negative values of $[H_2]_{INC}$–$[H_2]_{TD\text{-}next}$ suggest the presence of syntrophic coupling, while positive values and zero suggest its absence. The near-origin area is magnified in the insert. The error bar of the sample from the sulfate–methane transition zone (in Quadrant IV) delineates the range of $[H_2]_{EXT}$–$[H_2]_{TD\text{-}next}$ when the next most favorable terminal electron accepting process is set to be methanogenesis (right end) or acetogenic CO_2-reduction (left end). For the subsurface H_2 minimum at Site GeoB 12803, methanogenesis was considered the next most favorable terminal metabolism. Abbreviations: $[H_2]_{EXT}$ and $[H_2]_{INC}$, H_2 concentrations determined by the extraction and headspace equilibration methods, respectively; $[H_2]_{TD\text{-}next}$, H_2 concentration for the thermodynamically next most favorable terminal electron accepting process; LoD_m, methodological limit of detection of the extraction approach.

(1) The H_2 threshold concentration of terminal electron accepting processes increases in the order of iron and manganese reduction $\leqslant$ sulfate reduction $<$ methanogenesis $<$ acetogenic CO_2-reduction.
(2) Syntrophic coupling is present as long as a given mode of terminal metabolism maintains H_2 concentrations low enough to restrain the thermodynamically next most favorable process (Hoehler et al., 1998, 2001). We define $[H_2]_{TD}$ and $[H_2]_{TD\text{-next}}$ as the threshold H_2 concentrations of the thermodynamically most favorable and next most favorable terminal metabolism, which we deduced from pore water chemistry (for example, for sulfate-reducing sediment, $[H_2]_{TD\text{-next}}$ equals $[H_2]_{TD}$ of methanogenesis).
(3) During incubation it is assumed that syntrophic coupling of production and consumption of H_2 controls its concentration to the effect that $[H_2]_{TD} \leqslant [H_2]_{INC} < [H_2]_{TD\text{-next}}$ (cf. Hoehler et al., 1998).
(4) By analogy, $[H_2]_{TD} \leqslant [H_2]_{EXT} < [H_2]_{TD\text{-next}}$ is expected if syntrophic coupling controls concentrations of pore-water H_2 in situ. However, for the studied subseafloor sediments the LoD_m is only lower than the $[H_2]_{TD}$ for acetogenic CO_2-reduction at some depths (Fig. 4). Consequently, for the other processes the relationship between $[H_2]_{EXT}$ to $[H_2]_{TD}$ or $[H_2]_{TD\text{-next}}$ cannot be determined. Nevertheless, an observation of $[H_2]_{EXT} > LoD_m$ would support the absence of syntrophic coupling for those processes with $[H_2]_{TD\text{-next}}$ lower than the LoD_m, i.e., metal and sulfate reduction in our case.

For better comparison the data are categorized based on redox regimes and geochemical zonation (Fig. 6a) or incubation duration (Fig. 6b). In both figures, four quadrants are distinguished. In Quadrant I, $[H_2]_{INC} \geqslant [H_2]_{TD\text{-next}}$ and $[H_2]_{EXT} > LoD_m > [H_2]_{TD\text{-next}}$ suggest the absence of syntrophic coupling during incubation and in situ, while on the contrary in Quadrant III, $[H_2]_{INC} \leqslant [H_2]_{TD\text{-next}}$ and $[H_2]_{EXT} < LoD_m < [H_2]_{TD\text{-next}}$ indicate the presence of syntrophic coupling both during incubation and in situ. In Quadrant IV, no syntrophic coupling is observed in the incubation experiment ($[H_2]_{INC} \geqslant [H_2]_{TD\text{-next}}$) though it seems to control in situ concentrations ($[H_2]_{EXT} < LoD_m$). The opposite holds for Quadrant II, which represents the combination of syntrophy in vitro and its absence under in situ conditions. We considered this combination unlikely in nature and hence data falling into this quadrant are probably biased due to analytical problems. About 13% of our samples reside in Quadrant II, and more than half of them come from Site GeoB 12811 for which the time schedule of the cruise only allowed for 5 days of incubation.

With 77% of the samples plotting in Quadrants I and IV, syntrophic coupling seems to be largely weakened or absent during lab incubation. In Quadrant I sulfate-reducing sediment samples incubated for $\geqslant$11 days constitute the majority. Quadrant IV contains samples incubated for varied periods of time from iron reduction zone, sulfate reduction zone, sulfate-methane transition zone, and the organic-lean station GeoB 12815. The weakened syntrophic coupling in lab incubations can be explained by experimental conditions: (1) the sediments have not reached real steady states due to limited incubation time. This is conceivable as the low microbial activities in subseafloor sediment have been acknowledged (e.g., D'Hondt et al., 2002). (2) The incubation condition did not appropriately simulate the in situ condition, such as the high hydrostatic pressure or high in situ methane concentrations. Piezophilic bacteria isolated from deep-sea sediment are known to have growth rates that vary with pressure (Nogi et al., 2004; Arakawa et al., 2006). Deusner et al. (2010) also demonstrated that higher dissolved gas concentrations influenced the activities of some benthic prokaryotes. Incubation under high pressure, however, is technically challenging and difficult to implement for large batches of samples. For samples that plot in Quadrant IV, the observation of both $[H_2]_{INC} \geqslant [H_2]_{TD\text{-next}}$ and $[H_2]_{EXT} < LoD_m$ suggests that syntrophic coupling was probably present in situ but got lost in the lab incubation. However, for samples in Quadrant I, $[H_2]_{EXT} > LoD_m > [H_2]_{TD\text{-next}}$ suggests that syntrophic coupling was also weak or absent under in situ conditions, and the background-corrected $[H_2]_{EXT}$ values (up to 205 nmol L^{-1}) provide conservative estimates of dissolved H_2 in these samples.

The absence of thermodynamic control on H_2 level in iron-reducing sediment under in situ conditions is in line with the result of Hoehler et al. (1998), who observed that addition of metal oxides did not significantly change steady-state H_2 concentrations and attributed the finding to the insoluble nature of metallic electron acceptors. Nevertheless, the lack of close syntrophic coupling in sulfate-reducing sediment is unexpected. This would require that on the one hand, sulfate reducers are not sufficiently active to maintain low H_2 concentrations: Radiotracer measurements showed that sulfate reduction rates are much lower in deep-sea sediments (e.g., Knab et al., 2009) than in coastal sediments (e.g., Jørgensen and Parkes, 2010). On the other hand, there have to be H_2 sources that keep dissolved H_2 concentrations at high levels. Unfortunately, no rate measurements or modeling data are available for fermenting activities, making it difficult to assess whether an activity difference between fermentation and sulfate reduction is the explanation for the high H_2 levels. From the thermodynamic perspective, fermentation of volatile fatty acids (Table 3; $\Delta G = -15$ kJ mol^{-1} reaction), a common type of substrates for fermenting prokaryotes, can proceed without syntrophy only till 0.5–7.8 nmol L^{-1} of dissolved H_2 when the pore-water data of sulfate-bearing sediment at Site GeoB 12802 were used for calculation ($\alpha_{Butyrate} =$ 0.1–1 μmol L^{-1} (α is activity); $\alpha_{Propionate} =$ 0.1–1 μmol L^{-1}; $\alpha_{Acetate} =$ 1–10 μmol L^{-1}; $\alpha_{Bicarbonate} =$ 1–10 mmol L^{-1}; pH = 7.4). To explain the high background-corrected $[H_2]_{EXT}$ values, other sources of H_2 are needed. One possibility is the presence of other substrates whose fermentation has higher inhibitory H_2 levels (e.g., Elshahed and McInerney, 2001). The other possibility is H_2 of abiotic origins, such as pyrite precipitation (Drobner et al., 1990) or water radiolysis (Blair et al., 2007). Blair et al. (2007) estimated the average radiolytic H_2 yields of Peru Margin sediment to be around 1–2 $\times$ 10^{-12} mol yr^{-1} cm^{-3} sediment, equivalent to 1.4–2.9 nmol L^{-1} of dissolved H_2 per year when

porosity is set to 0.7. The significant H_2 yields and the fact that water radiolysis is not governed by thermodynamics make this abiotic process a plausible source for the high $[H_2]_{EXT}$ levels we observed.

Conditions in Quadrant III, which hosts 9% of the samples, suggest that the next most favorable terminal electron accepting process is restrained in the laboratory and probably also in situ. Three of the five samples showing this characteristic originate from the upper methanogenic zone at Site GeoB 12802. We were not able to quantify the loss of H_2 from methane-rich sediment during core retrieval, but both the samples taken immediately on deck and later in the cold room have $[H_2]_{EXT}$ lower than the LoD_m (Fig. 5). For incubation, flushing of headspace during sample handling (cf. Section 2.3.1) and the low incubation pressure highly reduced methane concentrations in the sediments. This probably explains why the $[H_2]_{INC}$ is often lower than the $[H_2]_{TD}$ for methanogenesis in this and previous studies (D'Hondt et al., 2003). Alternatively, methanogens can survive with lower amounts of energy. When the measured $[H_2]_{INC}$ of methanogenic sediment was used to calculate the ΔG values, we obtained energy yields as small as -9.0 ± 1.5 kJ mol^{-1} reaction, which are in accordance with the values determined for methanogenesis in coastal sediment (Hoehler et al., 2001).

4. CONCLUSIONS

Careful examination of the extraction method for H_2 determination in sediment samples revealed that the solution for preparing sediment slurry should be first equilibrated with atmosphere before use, and atmospheric H_2 leaking through septa during needle puncturing is a prominent source of background H_2. Optimization of the extraction method resulted in a reproducible LoD_m. Evaluation of the optimized method showed that above-LoD_m $[H_2]_{EXT}$, after subtraction of background H_2, underestimates the dissolved H_2 concentrations. Thus $[H_2]_{EXT}$ values above the LoD_m can be considered conservative estimates of sedimentary H_2 concentrations.

Previous studies applying either a headspace equilibration technique or an extraction method for the analysis of pore-water H_2 in subseafloor sediments have generated results that sometimes contradict the principles established based on studies of microbial culture and surface sediments. For the well established headspace equilibration technique, the low microbial activity and high pressure of deep-sea sediment make it difficult to assess whether a steady state is reached, and whether the incubation is carried out under conditions representative of in situ environments. Therefore, in this work, the extraction method and headspace equilibration technique were employed jointly to determine H_2 concentrations in subseafloor sediment. We demonstrated that with this joint approach, both data sets can be interpreted with greater confidence. Our results showed that a significant proportion of sediment samples with redox potential equal or higher than sulfate reduction have $[H_2]_{INC}$ concentrations higher than thermodynamically predicted values, and the corresponding $[H_2]_{EXT}$ data suggest that relaxation of coupling between H_2-producing and H_2-consuming activities may be taking place in situ in some of the sediments. In contrast, both $[H_2]_{INC}$ and $[H_2]_{EXT}$ data indicate that the next favorable terminal metabolism in methanogenic sediment, i.e., acetogenic CO_2-reduction, was restrained. This joint approach would be suitable for studying H_2 biogeochemistry in subseafloor sediment where microbial activities are expected to be low: The headspace equilibration technique provides information that can be discussed within the broader context of thermodynamics, whereas the extraction method provides a 'snapshot' of the in situ distribution that can be used in assistance to better understand the meaning of incubation-derived H_2 data.

ACKNOWLEDGEMENTS

We thank the captain and crew as well as the scientists on board the RV *Meteor* for their strong support during the cruises M 76/1 and M84/1. We thank T. Pape for sharing his invaluable experiences of gas analysis; S. Pape and S. Sauer for their help in pore-water analyses; T. Hörner, M.A. Lever, K. Becker, J. Schmal, N. Broda, M. Elvert for their help during sampling; J. Wendt for her competent work of H_2 analysis; T. Ferdelman and W. Bach for fruitful discussions. T. Ferdelman and G.L. Arnold are thanked for providing the sulfide data. We are grateful to D. Smith (URI) for his comments on an earlier version of this manuscript, and the three anonymous reviewers for their careful reviews. This study was supported by the DFG-Research Center/Cluster of Excellence 'The Ocean in the Earth System' (MARUM). Y.S.L. was co-sponsored by the Bremen International Graduate School for Marine Sciences (GLOMAR). The contribution of V.B.H. (participation in cruise and preparation of the manuscript) was supported by the Deutsche Forschungsgemeinschaft (project grants Hi 616/7-1, Hi 616/9-1). Data presented in this manuscript can be retrieved from the World Data Center for Marine Environmental Sciences at http://www.wdc-mare.org/.

APPENDIX A. SUPPLEMENTARY DATA

Supplementary data associated with this article can be found, in the online version, at doi:10.1016/j.gca.2011.11.008.

REFERENCES

Arakawa S., Nogi Y., Sato T., Yoshida Y., Usami R. and Kato C. (2006) Diversity of piezophilic microorganisms in the closed ocean Japan Sea. *Biosci. Biotechnol. Biochem.* **70**, 749–752.

Blair C. C., D'Hondt S., Spivack A. J. and Kingsley R. H. (2007) Radiolytic hydrogen and microbial respiration in subsurface sediments. *Astrobiology* **7**, 951–970.

Blum P. (1997) Physical properties handbook. *ODP Tech. Note 26*.

Cline J. D. (1969) Spectrofluorometric determination of hydrogen sulfide in natural waters. *Limnol. Oceanogr.* **14**, 454–458.

Conrad R. and Wetter B. (1990) Influence of temperature on energetics of hydrogen metabolism in homoacetogenic, methanogenic, and other anaerobic bacteria. *Arch. Microbiol.* **155**, 94–98.

Conrad R., Aragno M. and Seiler W. (1983) The inability of hydrogen bacteria to utilize atmospheric hydrogen is due to threshold and affinity for hydrogen. *FEMS Microbiol. Lett.* **18**, 207–210.

Conrad R., Phelps T. J. and Zeikus J. G. (1985) Gas metabolism evidence in support of the juxtaposition of hydrogen-producing

and methanogenic bacteria in sewage sludge and lake sediments. *Appl. Environ. Microbiol.* **50**, 595–601.

Cord-Ruwisch R., Seitz H. J. and Conrad R. (1988) The capacity of hydrogenotrophic anaerobic bacteria to compete for traces of hydrogen depends on the redox potential of the terminal electron acceptor. *Arch. Microbiol.* **149**, 350–357.

Crank J. (1975) *The Mathematics of Diffusion*. Oxford Univ. Press, Oxford.

Crozier T. E. and Yamamoto S. (1974) Solubility of hydrogen in water, seawater, and NaCl solutions. *J. Chem. Eng. Data* **19**, 242–244.

Deusner C., Meyer V. and Ferdelman T. G. (2010) High-pressure systems for gas-phase free continuous incubation of enriched marine microbial communities performing anaerobic oxidation of methane. *Biotechnol. Bioeng.* **105**, 524–533.

D'Hondt S., Rutherford S. and Spivack A. J. (2002) Metabolic activity of subsurface life in deep-sea sediments. *Science* **295**, 2067–2070.

D'Hondt S. L., Jørgensen B. B. and Miller D. J., et al. (2003) *Proc. ODP, Init. Repts., 201*. Ocean Drilling Program, College Station, TX.

D'Hondt S., Spivack A. J., Pockalny R., Ferdelman T. G., Fischer J. P., Kallmeyer J., Abrams L. J., Smith D. C., Graham D., Hasiuk F., Schrum H. and Stancin A. M. (2009) Subseafloor sedimentary life in the South Pacific Gyre. *Proc. Nat. Acad. Sci. U.S.A.* **106**, 11651–11656.

Drobner E., Huber H., Wächtershäuser G., Rose D. and Stetter K. O. (1990) Pyrite formation linked with hydrogen evolution under anaerobic conditions. *Nature* **346**, 742–744.

Elshahed M. S. and McInerney M. J. (2001) Benzoate fermentation by the anaerobic bacterium *Syntrophus aciditrophicus* in the absence of hydrogen-using microorganisms. *Appl. Environ. Microbiol.* **67**, 5520–5525.

Goldhammer T., Brunner B., Bernasconi S. M., Ferdelman T. G. and Zabel M. (2011) Phosphate oxygen isotopes: Insights into sedimentary phosphorus cycling from the Benguela upwelling system. *Geochim. Cosmochim. Acta* **75**, 3741–3756.

Hall P. O. J. and Aller R. C. (1992) Rapid, small-volume, flow injection analysis for $\sum CO_2$ and NH_4^+ in marine and freshwaters. *Limnol. Oceanogr.* **37**, 1113–1119.

Häring V. and Conrad R. (1991) Kinetics of H_2 oxidation in respiring and denitrifying *Paracoccus denitrificans*. *FEMS Microbiol. Lett.* **78**, 259–264.

Hedges J. I. and Keil R. G. (1995) Sedimentary organic matter preservation: an assessment and speculative synthesis. *Mar. Chem.* **49**, 81–115.

Heuer V., Elvert M., Tille S., Krummen M., Prieto Mollar X., Hmelo L. R. and Hinrichs K. U. (2006) Online $\delta^{13}C$ analysis of volatile fatty acids in sediment/porewater systems by liquid chromatography–isotope ratio mass spectrometry. *Limnol. Oceanogr.: Methods* **4**, 346–357.

Heuer V. B., Pohlman J. W., Torres M. E., Elvert M. and Hinrichs K. U. (2009) The stable carbon isotope biogeochemistry of acetate and other dissolved carbon species in deep subseafloor sediments at the northern Cascadia Margin. *Geochim. Cosmochim. Acta* **73**, 3323–3336.

Hoehler T. M., Alperin M. J., Albert D. B. and Martens C. S. (1998) Thermodynamic control on hydrogen concentrations in anoxic sediments. *Geochim. Cosmochim. Acta* **62**, 1745–1756.

Hoehler T. M., Albert D. B., Alperin M. J. and Martens C. S. (1999) Acetogenesis from CO_2 in an anoxic marine sediment. *Limnol. Oceanogr.* **44**, 662–667.

Hoehler T. M., Alperin M. J., Albert D. B. and Martens C. S. (2001) Apparent minimum free energy requirements for methanogenic Archaea and sulfate-reducing bacteria in an anoxic marine sediment. *FEMS Microbiol. Ecol.* **38**, 33–41.

Inagaki F., Nunoura T., Nakagawa S., Teske A., Lever M., Lauer A., Suzuki M., Takai K., Delwiche M., Colwell F. S., Nealson K. H., Horikoshi K., D'Hondt S. and Jørgensen B. B. (2006) Biogeographical distribution and diversity of microbes in methane hydrate-bearing deep marine sediments on the Pacific Ocean Margin. *Proc. Nat. Acad. Sci. U.S.A.* **103**, 2815–2820.

Inthorn M., Wagner T., Scheeder G. and Zabel M. (2006) Lateral transport controls distribution, quality and burial of organic matter along continental slopes in high-productivity areas. *Geology* **34**, 205–208.

Johnson J. W., Oelkers E. H. and Helgeson H. C. (1992) SUPCRT92: a software package for calculating the standard molal thermodynamic properties of minerals, gases, aqueous species, and reactions from 1 to 5000 bar and 0 to 1000 °C. *Comput. Geosci.* **18**, 899–947.

Jørgensen B. B. and Parkes R. J. (2010) Role of sulfate reduction and methane production by organic carbon degradation in eutrophic fjord sediments (Limforden, Denmark). *Limnol. Oceanogr.* **55**, 1338–1352.

Kelley D. S., Karson J. A., Früh-Green G. L., Yoerger D. R., Shank T. M., Butterfield D. A., Hayes J. M., Schrenk M. O., Olson E. J., Proskurowski G., Jakuba M., Bradetection limitey A., Larson B., Ludwig K., Glickson D., Buckman K., Bradley A. S., Brazelton W. J., Roe K., Elend M. J., Delacour A., Bernasconi S. M., Lilley M. D., Baross J. A., Summons R. E. and Sylva S. P. (2005) A serpentinite-hosted ecosystem: the Lost City hydrothermal field. *Science* **307**, 1428–1434.

Klüber H. D. and Conrad R. (1993) Ferric iron-reducing *Shewanella putrefaciens* and N_2-fixing *Bradyrhizobium japonicum* with uptake hydrogenase are unable to oxidize atmospheric H_2. *FEMS Microbiol. Lett.* **111**, 337–342.

Knab N. J., Cragg B. A., Hornibrook E. R. C., Holmkvist L., Pancost R. D., Borowski C., Parkes R. J. and Jørgensen B. B. (2009) Regulation of anaerobic methane oxidation in sediments of the Black Sea. *Biogeosciences* **6**, 1505–1518.

Kotsyurbenko O. R., Glagolev M. V., Nozhevnikova A. N. and Conrad R. (2001) Competition between homoacetogenic bacteria and methanogenic archaea for hydrogen at low temperature. *FEMS Microbiol. Ecol.* **38**, 153–159.

Krämer H. and Conrad R. (1993) Measurement of dissolved H_2 concentrations in methanogenic environments with a gas diffusion probe. *FEMS Microbiol. Ecol.* **12**, 149–158.

Krumholz L. R., Harris S. H., Tay S. T. and Suflita J. M. (1999) Characterization of two subsurface H_2-utilizing bacteria, *Desulfomicrobium hypogenium* sp. nov. and *Acetobacterium psammolithicum* sp. nov., and their ecological roles.. *Appl. Environ. Microbiol.* **65**, 2300–2306.

Kvenvolden K. A. and McDonald T. J. (1986) Organic geochemistry on the JOIDES Resolution—an essay. *ODP Tech. Note 6*.

Lever M. A., Heuer V. B., Morono Y., Masui N., Schmidt F., Alperin M. J., Inagaki F., Hinrichs K. U. and Teske A. (2010) Acetogenesis in deep subseafloor sediments of the Juan de Fuca Ridge Flank: a synthesis of geochemical, thermodynamic, and gene-based evidence. *Geomicrobiol. J.* **27**, 183–211.

Lovley D. R. (1985) Minimum threshold for hydrogen metabolism in methanogenic bacteria. *Appl. Environ. Microbiol.* **49**, 1530–1531.

Lovley D. R. and Goodwin S. (1988) Hydrogen concentrations as an indicator of the predominant terminal electron-accepting reactions in aquatic sediments. *Geochim. Cosmochim. Acta* **52**, 2992–3003.

Lovley D. R., Phillips E. J. P. and Lonergan D. J. (1989) Hydrogen and formate oxidation coupled to dissimilatory reduction of iron or manganese by *Alteromonas putrefaciens*. *Appl. Environ. Microbiol.* **55**, 700–706.

Martens C. S. and Berner R. A. (1974) Methane production in the interstitial waters of sulfate-depleted marine sediments. *Science* **27**, 1167–1169.

Michener R. H., Scranton M. I. and Novelli P. (1988) Hydrogen (H_2) distributions in the Carmans River Estuary. *Estuar. Coast. Shelf Sci.* **27**, 223–235.

Nogi Y., Hosoya S., Kato C. and Horikoshi K. (2004) *Colwellia piezophila* sp. nov., a novel piezophilic species from deep-sea sediments of the Japan Trench. *Int. J. Syst. Evol. Microbiol.* **54**, 1627–1631.

Novelli P. C., Scranton M. I. and Michener R. H. (1987) Hydrogen distributions in marine sediments. *Limnol. Oceanogr.* **32**, 565–576.

Novelli P. C., Michelson A. R., Scranton M. I., Banta G. T., Hobbie J. E. and Howarth R. W. (1988) Hydrogen and acetate cycling in two sulfate-reducing sediments: Buzzards Bay and Town Cove, Mass. *Geochim. Cosmochim. Acta* **52**, 2477–2486.

Novelli P. C., Lang P. M., Masarie K. A., Hurst D. F., Myers R. C. and Elkins J. W. (1999) Molecular hydrogen in the troposphere: global distribution and budget. *J. Geophys. Res.* **104**, 30427–30444.

Parkhurst D. L. and Appelo C. A. J. (1999) User's guide to PHREEQC (version 2)—a computer program for speciation, batch-reaction, one-dimensional transport, and inverse geochemical calculations. *U.S. Geological Survey Water Resources Investigations Report 99-4259*, U.S. Geological Survey, Denver, CO.

Pauly S. (1989) Permeability and diffusion data. In *Polymer Handbook* (eds. J. Brandup and E. H. Immergut). John Wiley and Sons, Oxford, pp. 435–446.

Pohlman J. W., Kaneko M., Heuer V. B., Coffin R. B. and Whiticar M. (2009) Methane sources and production in the northern Cascadia margin gas hydrate system. *Earth Planet. Sci. Lett.* **287**, 504–512.

Schink B. and Stams A. J. M. (2006) Syntrophism among prokaryotes. *The Prokaryotes* **2**, 309–335.

Schippers A., Neretin L. N., Kallmeyer J., Ferdelman T. G., Cragg B. A., Parkes R. J. and Jørgensen B. B. (2005) Prokaryotic cells of the deep sub-seafloor biosphere identified as living bacteria. *Nature* **433**, 861–864.

Seeberg-Elverfeldt J., Schluter M., Feseker T. and Kölling M. (2005) Rhizon sampling of porewaters near the sediment-water interface of aquatic systems. *Limnol. Oceanogr.: Methods* **3**, 361–371.

Seewald J. S. (2003) Organic–inorganic interactions in petroleum-producing sedimentary basins. *Nature* **426**, 327–333.

Shock E. L. and Helgeson H. C. (1990) Calculation of the thermodynamic and transport properties of aqueous species at high pressures and temperatures: standard partial molal properties of organic species. *Geochim. Cosmochim. Acta* **54**, 915–945.

Souers P. C., Moen I., Lindahl R. O. and Tsugawa R. T. (1978) Permeation eccentricities of He, Ne, and D-T from soda-lime glass microbubbles. *J. Am. Ceram. Soc.* **61**, 42–46.

Sowers K. R. and Ferry J. G. (1983) Isolation and characterization of a methylotrophic marine methanogen, *Methanococcoides methylutens* gen. nov., sp. nov.. *Appl. Environ. Microbiol.* **45**, 684–690.

Spivack A. J., Kastner M. and Ransom B. (2002) Elemental and isotopic chloride geochemistry and fluid flow in the Nankai Trough. *Geophys. Res. Lett.* **29**. doi:10.1029/2001GL014122.

Stams A. J. M. and Plugge C. M. (2009) Electron transfer in syntrophic communities of anaerobic bacteria and archaea. *Nature Rev. Microbiol.* **7**, 568–577.

Teske A. P. (2006) Microbial communities of deep marine subsurface sediments: molecular and cultivation surveys. *Geomicrobiol. J.* **23**, 357–368.

Weisenberger S. and Schumpe A. (1996) Estimation of gas solubilities in salt solutions at temperatures from 273 K to 363 K. *AIChE J.* **42**, 298–300.

Associate editor: Susan Glasauer